COLD SPRING HARBOR
Molecular Case Studies

RESEARCH REPORT

Molecular and clonal evolution in recurrent metastatic gliosarcoma

Kevin J. Anderson,[1,8] Aaron C. Tan,[2,3,8] Jonathon Parkinson,[2,4,5] Michael Back,[2,4,5] Marina Kastelan,[2,4] Allison Newey,[2] Janice Brewer,[2] Helen Wheeler,[2,4,5,6] Amanda L. Hudson,[2,4,5,6] Samirkumar B. Amin,[1] Kevin C. Johnson,[1] Floris P. Barthel,[1,7] Roel G.W. Verhaak,[1,9] and Mustafa Khasraw[2,4,5,9]

[1]The Jackson Laboratory for Genomic Medicine, Farmington, Connecticut 06085, USA; [2]Royal North Shore Hospital, Northern Sydney Local Health District, St Leonards, New South Wales 2065, Australia; [3]National Cancer Centre Singapore, Singapore, 169610 Singapore; [4]The Brain Cancer Group, North Shore Private Hospital, St Leonards, New South Wales 2065, Australia; [5]The NHMRC Clinical Trials Centre, the University of Sydney, Camperdown, New South Wales 2066, Australia; [6]Bill Walsh Translational Cancer Research Laboratory, Kolling Institute of Medical Research, St Leonards, New South Wales 2065, Australia; [7]Department of Pathology, VU University Medical Center/Brain Tumor Center Amsterdam, Amsterdam 1081 HV, The Netherlands

Abstract We discuss the molecular evolution of gliosarcoma, a mesenchymal type of glioblastoma (GBM), using the case of a 37-yr-old woman who developed two recurrences and an extracranial metastasis. She was initially diagnosed with isocitrate dehydrogenase (IDH) wild-type gliosarcoma in the frontal lobe and treated with surgery followed by concurrent radiotherapy with temozolomide. Five months later the tumor recurred in the left frontal lobe, outside the initially resected area, and was treated with further surgery and radiotherapy. Six months later the patient developed a second left frontal recurrence and was again treated with surgery and radiotherapy. Six weeks later, further recurrence was observed in the brain and bone, and biopsy confirmed metastases in the pelvic bones. To understand the clonal relationships between the four tumor instances and the origin of metastasis, we performed whole-genome sequencing of the intracranial tumors and the tumor located in the right iliac bone. We compared their mutational and copy-number profiles and inferred the clonal phylogeny. The tumors harbored shared alterations in GBM driver genes, including mutations in *TP53*, *NF1*, and *RB1*, and *CDKN2A* deletion. Whole-genome doubling was identified in the first recurrence and the extracranial metastasis. Comparisons of the metastatic to intracranial tumors highlighted a high similarity in molecular profile but contrasting evidence regarding the origin of the metastasis. Subclonal reconstruction suggested a parallel evolution of the recurrent tumors, and that the metastatic tumor was largely derived from the first recurrence. We conclude that metastasis in glioma can be a late event in tumorigenesis.

[Supplemental material is available for this article.]

INTRODUCTION

Glioblastoma (GBM), a World Health Organization grade IV glioma, is the most common malignant brain tumor in adult patients and is associated with extremely poor prognosis (Weller et al. 2015). Despite standard treatment of surgical resection followed by concomitant

Corresponding author:
mustafa.khasraw@sydney.edu.au

Ontology terms: glioblastoma; glioma; IDH; neoplasm of the nervous system

Published by Cold Spring Harbor Laboratory Press

doi:10.1101/mcs.a004671

[8]These authors contributed equally to this work.
[9]Co-senior authors

radiation and chemotherapy, recurrence is considered inevitable. As a result, patients with GBM currently have a median survival of only 15 mo (Parsons et al. 2008; Weller et al. 2015; Ostrom et al. 2016). This poor prognosis is due, in part, to the diffusive invasive growth of GBM cells, which prevents the possibility of complete resection and limits the effect of local radiotherapy (Naumman et al. 2013; Memmel et al. 2017). Poor prognosis can also be attributed to large inter- and intratumoral heterogeneity, wherein tumor subpopulations associated with different molecular characteristics develop resistance to radiation and chemotherapies (Liu et al. 2018; Akgül et al. 2019). Various molecular characteristics have been associated with distinct GBM subtypes, and studies have increasingly shown that molecular profiling can be used to identify clinically relevant tumor subtypes and aid in treatment decisions (Verhaak et al. 2010; Ceccarelli et al. 2016; Barthel et al. 2018).

Here we present a case of a 37-yr-old woman who was diagnosed with isocitrate dehydrogenase wild-type (IDHwt) gliosarcoma and developed local and distant recurrences, including extracranial metastases to the vertebral and pelvic bones. Gliosarcoma is a variant of GBM that contains distinct glial and mesenchymal components. Histologically, the glial component matches criteria for GBM, and the mesenchymal component displays a variety of phenotypes. Both components of gliosarcoma share genetic alterations common to GBM, including gains in Chromosomes 7, 20q, and X and losses in Chromosomes 9p, 10, and 3q. Both components also commonly contain *PTEN* and *TP53* mutations, *CDKN2A* deletion, and *EGFR*, *MDM2*, and *CDK4* amplifications (Han et al. 2010; Codispoti et al. 2014).

Although GBM is known to strongly infiltrate surrounding tissue, extracranial metastases are rare, with a reported incidence of <2% (Kalokhe et al. 2012), gliosarcoma may have a greater propensity compared to GBM (Dawar et al. 2013). Although studies have investigated potential causes for extracranial metastases, the mechanism is still poorly understood, and data is limited (Waite et al. 1999; Kalokhe et al. 2012; Rosen et al. 2018). Using high-coverage whole-genome sequencing (WGS) of four spatially and temporally distinct samples, we investigated the relationship between the metastases and intracranial tumors in order to study the impact of genetic alterations in primary tumors on tumor progression and metastasis and identify potential targets for therapeutic intervention.

RESULTS

Case Presentation

A 37-yr-old Caucasian woman initially presented with headaches and unsteady gait. She had a past history of secondary atrioventricular block and was on no regular medications. Magnetic resonance imaging (MRI) of the brain revealed a 55 × 45 × 56-mm mass lesion within the left frontal lobe, demonstrating an irregular rim of peripheral marginal enhancement and central cystic change (Fig. 1A). There was prominent surrounding white matter edema, mass effect with effacement of the anterior horn of the left lateral ventricle. The patient underwent a craniotomy and complete resection, with histopathology showing microscopic appearance and immunohistochemistry consistent with gliosarcoma (Fig. 1E). The biopsied sample showed positive staining for glial fibrillary acidic protein (GFAP), vimentin, P53, and synaptophysin, with Ki67 positive staining in up to 65% of tumor cells. There was a biphasic pattern of growth with spindle cell areas associated with reticulin deposition and loss of GFAP positivity. The sample showed negative staining for IDH1 R132H (c.395G > A) and BRAF V600E (c.1799T > A). *MGMT* promoter methylation was also assessed, and it was found to be unmethylated. The patient commenced 60 Gy in 30 fractions radiotherapy with temozolomide (TMZ) and was also enrolled in a clinical trial investigating the addition

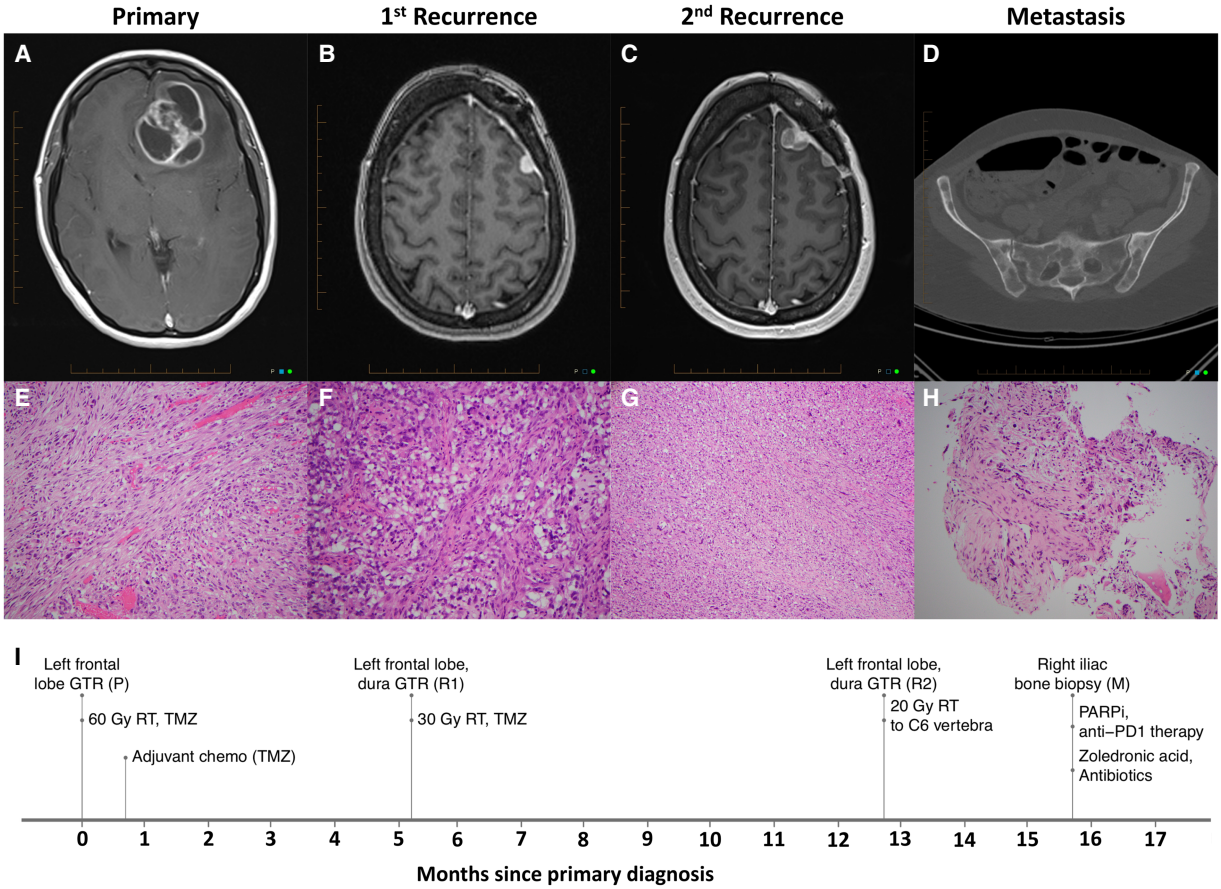

Figure 1. Clinical presentation of metastatic gliosarcoma. (*A–C*) Magnetic resonance imaging (MRI) of initial tumor diagnosis for the primary (P), first recurrent (R1), and second recurrent (R2) tumors, respectively. (*D*) Computed tomography (CT) scan of initial diagnosis of metastatic (M) tumor. (*E–H*) Hematoxylin and eosin stain of biopsy specimens from tumors P, R1, R2, and M, respectively. (*I*) Timeline of patient diagnoses and treatments. Sample designations are denoted in parentheses after the procedure they were collected from. (GTR) Gross tumor resection, (RT) radiotherapy, (TMZ) temozolomide.

of nivolumab or placebo. Following the chemoradiation treatment, she completed one cycle of further adjuvant chemotherapy with TMZ (Fig. 1I).

A follow-up MRI showed stable postoperative changes at the resection site, however a new extra-axial homogenously enhancing nodule was found at the posterosuperior margin of the craniotomy, outside the previous radiation field, measuring 12 × 7 mm (Fig. 1B). MRI of the spine showed no evidence of spinal metastases. Preoperative imaging 2 wk after the recurrence was initially observed showed the lesion had increased to 16 × 14 mm. The patient subsequently underwent a further craniotomy and resection, with histopathology revealing recurrent gliosarcoma (Fig. 1F), similarly showing a high-grade glial tumor displaying a biphasic pattern of growth. The tumor sections comprised components of pleomorphic mitotically active spindle cells, associated with reticulin deposition, which formed a meshwork intersecting islands of malignant glial forms. Further radiotherapy (30 Gy in fractions) was given postoperatively to the resection cavity.

On follow-up MRI 6 mo later, two further extra-axial masses with adjacent edema of the left frontal lobe were detected measuring 20 and 11 mm, within and outside the radiotherapy field, respectively (Fig. 1C). She was asymptomatic of her recurrence and proceeded to

further resection, with histopathology confirming further recurrent gliosarcoma (Fig. 1G). Interestingly there was loss of staining of GFAP in many areas of the tumor including the glial component and not just the sarcomatous component. Bizarre tumor giant cells were more conspicuous than in the previous resection specimens with atypical mitoses also noted. Postoperative MRI 6 wk later revealed further recurrent disease with a nodule in the left inferior frontal lobe measuring 17 mm, irregular nodular enhancement more superiorly involving the left frontal lobe measuring 23 mm, and irregular smaller areas of enhancement extending deep into the brain. Whole-spine MRI and CT demonstrated widespread marrow involvement of all vertebrae (Fig. 1D). Palliative radiotherapy of 20 Gy in five fractions was given to the C6 lesion, and the patient was referred for another clinical trial involving molecular profiling for targeted treatment. The tumor tissue from her second resection was found to have *RAD51*, *FANCE*, and *CDK12* homozygous loss. She was therefore commenced on a PARP inhibitor in combination with anti-PD-1 immune checkpoint inhibitor therapy on a clinical trial. A biopsy of the right iliac bone was also performed, with histopathology revealing morphological features similar to the previously resected gliosarcoma (Fig. 1H). Immunohistochemistry was also consistent with gliosarcoma; the sample showed positive staining for vimentin in all components and selective positivity for GFAP with strong positive staining of tumor cells in a viable hypercellular focus and lack of staining of dispersed atypical spindled cells in adjacent collagenous stroma.

One week after completing her palliative radiotherapy, she was admitted to hospital with hypercalcemia (corrected calcium 4.08 mmol/L) and treated with intravenous fluid rehydration and zoledronic acid. Her admission was also complicated by recurrent fevers due to a lower respiratory tract infection, which was treated with intravenous antibiotics. She was discharged after 15 d and later died. A timeline of the patient's diagnoses and treatments is illustrated in Figure 1I.

Genomic Analyses

To understand the pattern of tumor evolution between the cranial lesions and the extracranial metastasis, we generated WGS data with a mean coverage of ≈70× for the primary (P), first recurrence (R1), second recurrence (R2), and extracranial metastasis (M) tumors (Supplemental Table 1) and a matching germline sample. The union of somatic variants identified across all four tumor samples was 13,970, of which 622 were in protein-coding regions (Table 1). Of the total variants detected, 5447 (39%) were shared across all samples, confirming their clonal relationship and supporting the diagnosis of the bony lesion as an extracranial metastasis derived from the primary brain tumor (Fig. 2A). Of the remaining variants, 4113 (29%) were shared between two or three samples, and the remaining 4410 (32%) were sample-specific. The mutational frequency of the primary tumor, 2.73 mutations/megabase (Mb), was comparable to the median mutational frequency previously reported for GBM (Lawrence et al. 2013) and was increased in recurrent tumors relative to the primary. The mutational frequency was highest for R2 (4.05 mutations/Mb), with R1 and M tumors having similar mutational frequencies (3.09 and 3.11 mutations/Mb, respectively).

Somatic mutations in the tumors were compared against a list of driver events determined through dN/dScv analysis, as described in Martincorena et al. (2017), of positively selected mutations in the Glioma Longitudinal AnalySiS (GLASS) Consortium cohort (Barthel et al. 2019). All four tumors shared mutations in *TP53*, *NF1*, and *RB1* and homozygous deletions of *CDKN2A* (Fig. 2B). The *TERT* promoter mutation C228T was reported for the primary, first recurrent sample, and second recurrent sample. Thirty-one sequencing reads were observed at the *TERT* C228T locus for the metastatic sample, and of them two reads carried the alternate allele, which is below the threshold for a mutation to be called by Mutect2. However, considering known challenges with identification of *TERT* promoter

Table 1. Variants identified from genomic profiling

Gene	Chromosome	HGVS DNA reference	HGVS protein reference	Variant type	Predicted effect (substitution, deletion, etc.)	dbSNP/dbVar ID	Genotype (heterozygous/ homozygous)
NF1	17	c.6992_7006del	p.Tyr2331_ Ala2336delinsSer	Inframe deletion	Deletion	N/A	Heterozygous
RB1	13	N/A	N/A	Upstream gene variant	Deletion	N/A	Heterozygous
RB1	13	c.795del	p.Lys265AsnfsTer3	Frameshift variant	Deletion	N/A	Heterozygous
TERT	5	g.1295228G > A	N/A	Upstream gene variant	Substitution	rs1242535815	Heterozygous
TP53	17	c.725G > A	p.Cys242Tyr	Missense mutation	Substitution	rs121912655	Heterozygous
QKI	6	c.287T > C	p.Phe96Ser	Missense mutation	Substitution	N/A	Heterozygous

variants with WGS (Colebatch et al. 2018), the prevalence of *TERT* promoter mutations in GBM (Ceccarelli et al. 2016), and the presence of the mutations in the other samples, it is likely that the metastatic sample harbors this mutation as well. Targeted sequencing would be required to confirm the presence of the mutation. This distinction of R2 from the other recurrent tumors with respect to mutational frequency is reflected in the presence of a missense mutation in *QKI* shared only in the primary tumor.

Analysis of sample mutational profiles showed a high contribution of Catalog of Somatic Mutations in Cancer (COSMIC) mutational signatures 1, 3, 8, and 16 to all tumors sampled (Fig. 3A). Signature 1 activity is characterized by C > T mutations at CpG dinucleotides, and the number of those mutations correlates with the age of diagnosis (Alexandrov et al. 2013, 2015). Signature 3 has been associated with defective DNA double-strand break repair, and in a subset of cancers this signature was strongly associated with *BRCA1/2* mutations (Alexandrov et al. 2013). However, no mutations in *BRCA1*, *BRCA2*, or the associated genes *PALB2* and *RAD51* were detected in either the primary or recurrent tumors. The etiology of signatures 8 and 16 remains unknown, but the activity of these signatures possibly

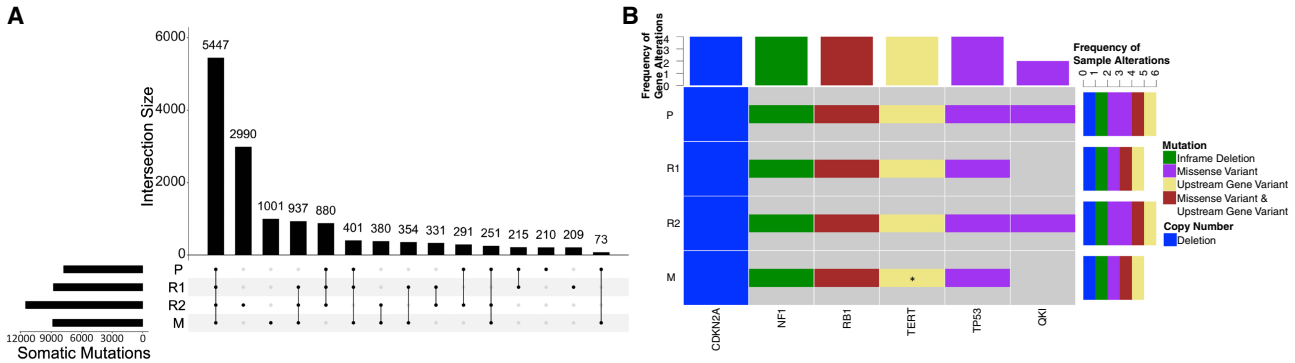

Figure 2. Comparative distribution of alterations among primary and recurrent tumors. (*A*) Upset plot of somatic mutations present in tumor samples. (*B*) Heatmap of mutations and focal copy-number alterations in glioma driver genes. An asterisk denotes mutation detection with insufficient coverage.

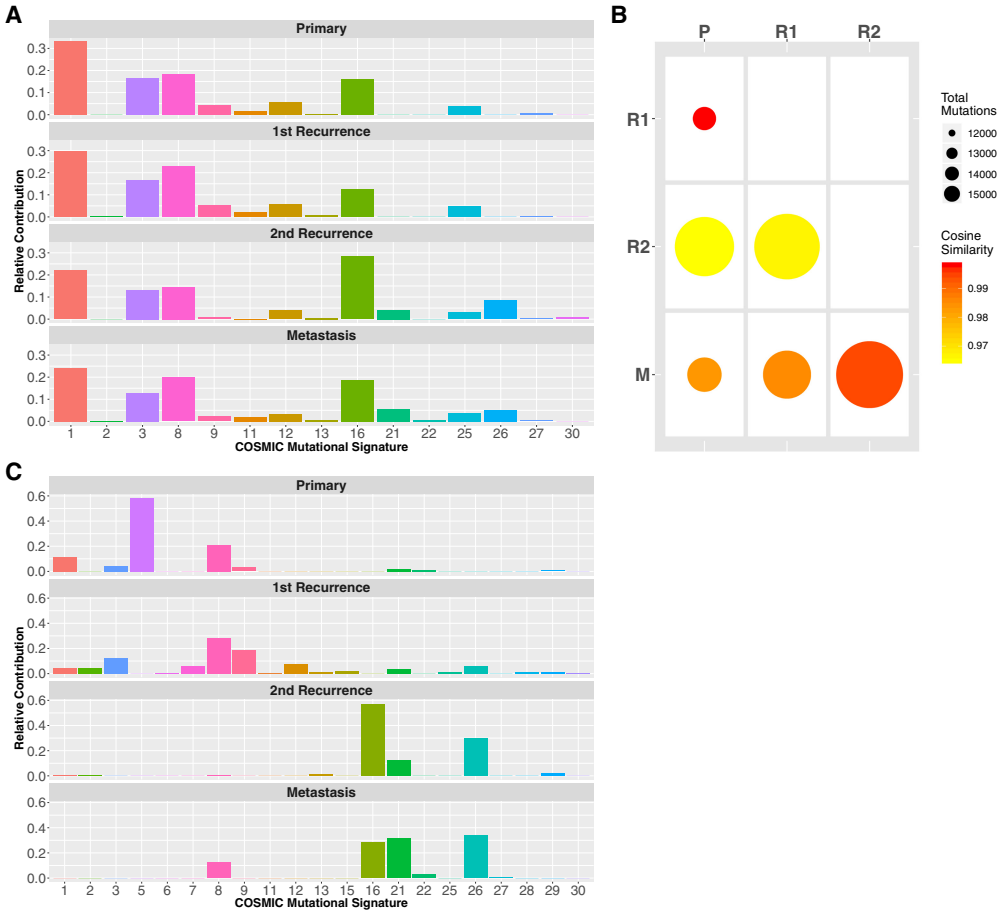

Figure 3. Mutational signature profiles of primary and recurrent tumors. (*A*) Barplot of the relative contribution of COSMIC signatures derived from all mutations. (*B*) Heatmap of pairwise cosine similarity of mutational signatures derived from all mutations. The size of the circle correlates with the total number of mutations present in the tumor pairs, and the circle color correlates with the cosine similarity value for the given tumor pair. (*C*) Barplot of the relative contribution of COSMIC signatures derived from mutations private to a single sample.

reflects DNA damage processed by transcription-coupled nucleotide excision repair (Alexandrov et al. 2013). Signature 11 activity, which is associated with TMZ treatment (Alexandrov et al. 2013), was negligible in all samples, suggesting that TMZ treatment did not appreciably contribute to the mutational load in this patient.

To quantify the similarity of the tumor mutational profiles, the mutational profiles of each combination of tumor pairs were compared using the cosine similarity metric, which evaluates the similarity in the relative frequency of base substitutions in the trinucleotide context (Fig. 3B; Blokzijl et al. 2018). The cosine similarity among all tumor pairs was high, with reported cosine similarity values of >0.96.

The P-R1 tumor pair had the highest cosine similarity (0.998), which was expected given the relative timing and mutational burden of the tumors. The cosine similarity for tumor pairs involving the metastatic tumor was >0.98 and was highest for the R2–M pair, suggesting that in terms of mutational profiles the metastatic tumor was most similar to R2. This is reflected in the footprints of mutations signatures 21 and 26, derived from the COSMIC database (Alexandrov et al. 2013, 2015), that were observed only in the R2 and M tumors; these

signatures have been associated with defective DNA mismatch repair. Restricting mutational signature analysis to mutations private to each sample, it was observed that signature 21 and 26 mutations comprised 42% and 65% of the private mutations in R2 and M, respectively (Fig. 3C). Comparison of the private mutational profiles highlights the activity of signatures with high contributions to samples R2 and M but a negligible contribution to samples P and R1 and vice versa.

Ionizing radiation was administered as treatment, and studies have shown that DNA damage from ionizing radiation can increase indel mutational burden and induce secondary malignancies (Behjati et al. 2016). For tumors significantly influenced by ionizing radiation, enrichment of deletions and insertions was uneven, resulting in an excess of deletions. The genome-wide ratio of deletion/insertion burden was measured for the primary and intracranial recurrent tumors, and it was found to be higher in the primary than recurrent tumors (data not shown). This suggests that ionizing radiation was not a significant contributor to malignant progression.

A previous study of gliosarcomas found that they share several copy-number alterations classically seen in GBM, but the number of chromosomes involved in alterations was significantly lower (Actor et al. 2002). However, evaluation of copy-number profiles in these tumors showed a high number of chromosomes with alterations, with variable alteration consistency across tumors (Fig. 4A). Homozygous deletion of Chromosome 9p21.3, the region overlapping *CDKN2A/CDKN2B*, is one of the few GBM copy-number alterations that was consistent across all samples. Chromosome 7 gain coupled with 10 loss (+7/−10), a common event in IDH wild-type glioma, was not observed in any sample. This was not considered atypical, as +7/−10 is observed in 66.7% of IDH wild-type gliomas (Ceccarelli et al. 2016). Among the recurrent tumors, *TP53* loss of heterozygosity (LOH) was observed for R1, R2, and M. R2 and M also displayed LOH for *RB1*. Samples R1 and M displayed widespread amplifications indicative of whole-genome doubling (Bielski et al. 2018). A major copy number of 2 or more was exhibited by 66.44% and 53.73% of the autosomal genome for R1 and M, respectively. The copy-number profile of sample R2 was distinct from other tumors in the presence of oscillations in chromosome segment copy number, similar to chromothripsis events (Luijten et al. 2018) or extrachromosomal DNA amplifications (deCarvalho et al. 2018).

To quantify the extent of similarity in copy-number alterations between the primary and recurrent tumors, chromosome arm-level aneuploidy scores were calculated using the methods described in Taylor et al. (2018). Copy-number segments generated by Sequenza for the p and q arms of nonacrocentric autosomes along with the q arms of acrocentric Chromosomes 13–15, 21, and 22 were aggregated and designated as gain, loss, or neutral based on their copy-number relative to the tumor ploidy. Aggregated segments that spanned at least 80% of the arm were considered arm-level events and given a score of 1, −1, or 0 for arm-level gain, loss, or neutrality, respectively. These scores were used to estimate the fraction of aneuploid genome, which was 0.3151, 0.4481, 0.8289, and 0.2628 for samples P, R1, R2, and M, respectively. The distribution of segment copy number was compared for each combination of tumor pairs (Fig 4B). The distribution of segment copy number for P showed low correlation with tumors R2 and M, but a higher similarity was observed between recurrent tumors. This is partially attributed to the increase in altered copy-number segments in recurrent tumors relative to the primary. The tumor pair with the highest Spearman's correlation coefficient observed was between tumors R1 and M, which was expected given those tumors were the only two having undergone genome doubling. Mutational signature profile similarity was not consistent with genome-wide copy-number similarity for any tumor pair; despite a relatively high overall similarity in mutational signatures among tumor pairs, copy-number similarity varied greatly.

Somatic mutation profiles, copy-number profiles, and tumor purity estimates were integrated in order to infer the subclonal population structure of the tumors. Using PhyloWGS

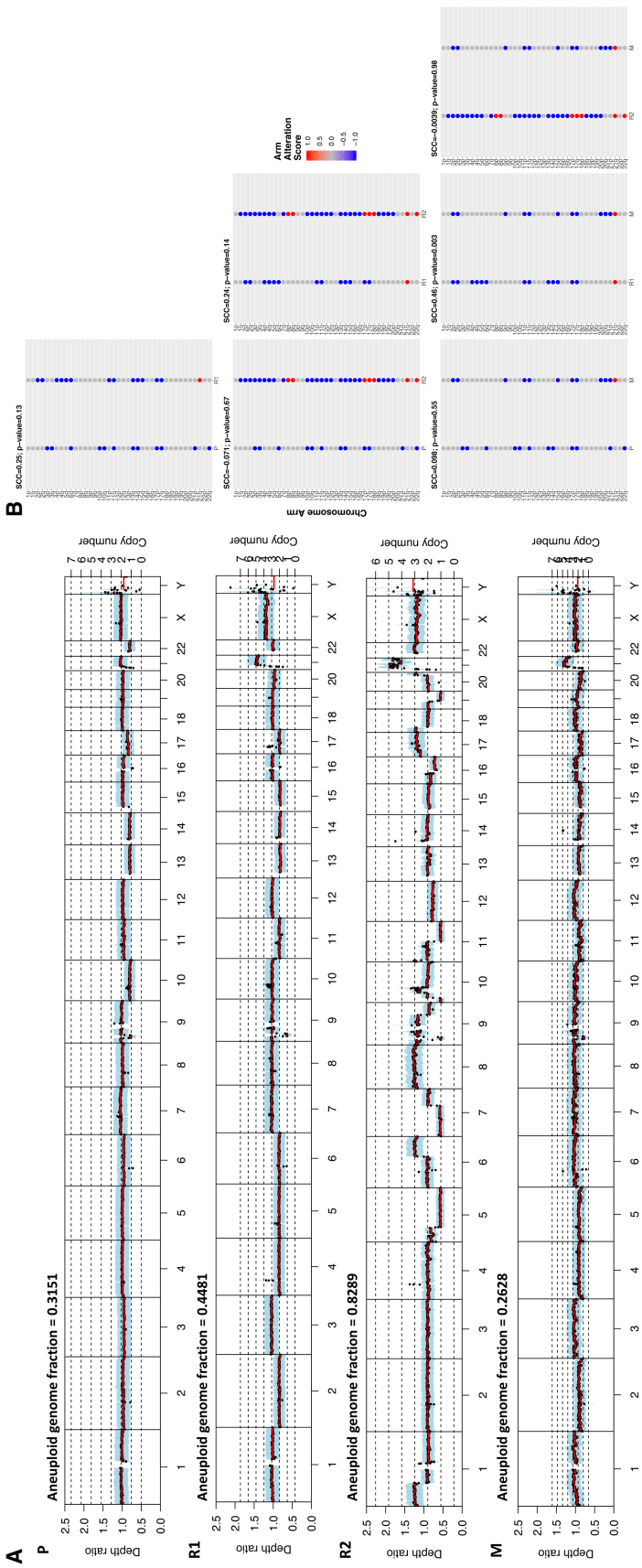

Figure 4. Copy-number alterations in primary and recurrent tumors. (*A*) Copy-number profiles of tumor samples as estimated by Sequenza. Copy number is reported as depth ratio, in which a depth ratio of 1 corresponds to a total copy-number equal to the tumor ploidy. Sequenza estimates of tumor ploidy were 1.9, 2.8, 2.3, and 2.5 for tumors P, R1, R2, and M, respectively. (*B*) Pairwise comparisons of arm-level aneuploidy scores, as calculated by the Taylor et al. method (Taylor et al. 2018). A given chromosome arm was considered aneuploid if ≥80% was altered in the same direction. Chromosome arms were given a score of +1 for copy-number gain, −1 for copy-number loss, and 0 otherwise. For each subpanel, the tumor with the earliest diagnosis of the pair is on the left. Spearman's correlation coefficient was calculated for the aneuploidy scores of each tumor pair and is reported above each subfigure. The aneuploid genome fraction was calculated by summing the length of all altered chromosome arms and dividing by the length of the genome.

(Deshwar et al. 2015), somatic SNV mutations (sSNVs) were clustered based on variant allele frequency in order to determine sSNV population frequencies, with corrections for sSNVs overlapping copy-number alterations. These variant allele frequency clusters correspond to subclonal lineages that are used to infer the clonal architecture of one or more tumors from a given patient. This approach results in the generation of multiple valid phylogenies, but for analysis the highest scoring phylogenetic tree, based on lowest negative normalized log likelihood, was chosen. The top scoring tree consisted of 13 clones containing 2346 sSNVs and 36 copy-number alterations, and for each clone the variant population cancer cell fraction (CCF) was inferred for each tumor (Fig. 5). Results of subclonal reconstruction suggest a branched evolution pattern, which has been previously observed in GBM and other tumor types (Brastianos et al. 2015; Barthel et al. 2019). Also consistent with previous

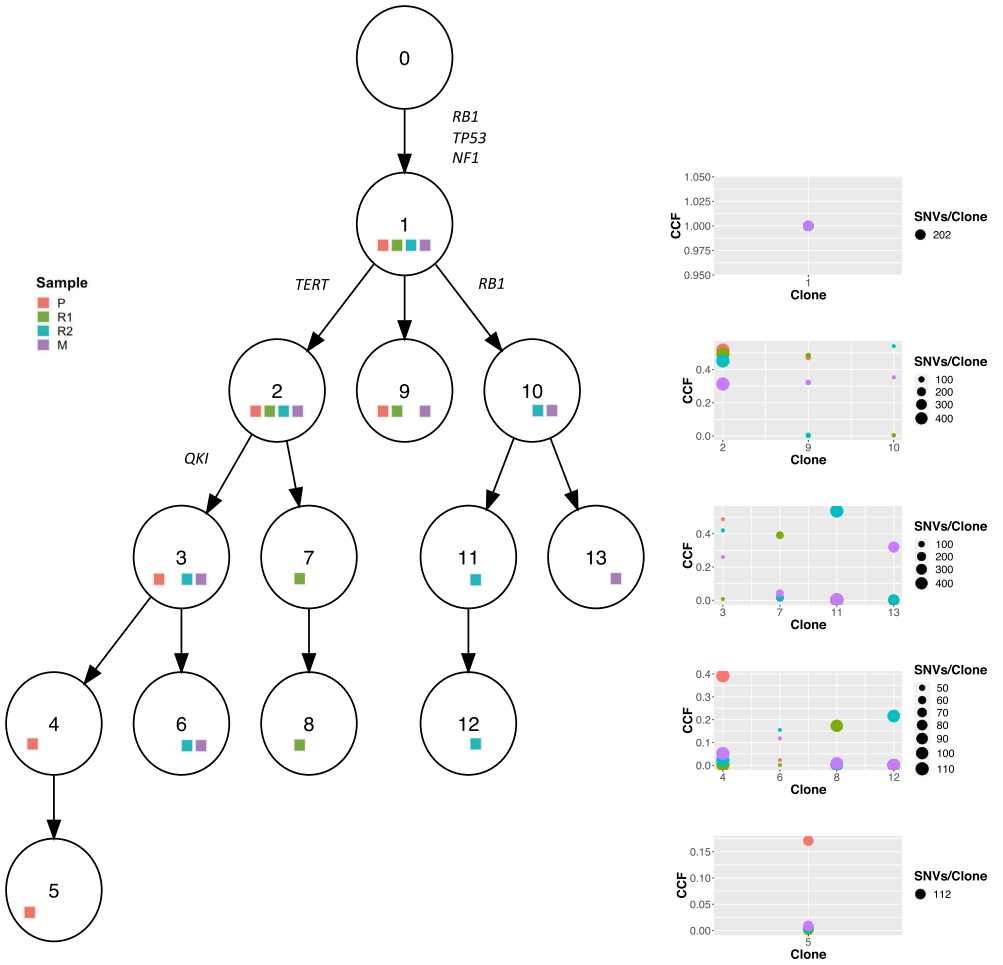

Figure 5. Subclonal composition of primary and recurrent tumors. Phylogenetic tree inferred by PhyloWGS from copy-number, somatic variant, and tumor purity data for patient primary (P) and recurrent (R1, R2, M) samples. Clonal evolution progresses from *top* to *bottom*, with each row representing a clonal generation. Each numbered node corresponds to a set of acquired mutations, which represents a tumor clone. Acquired mutations on driver genes are annotated on tree branches. Colored squares within each node denote samples for which the clone cancer cell fraction (CCF) is >0.1. Sample clone CCFs are depicted to the right of each generation. The thickness of the points correspond to the number of single-nucleotide variants (SNVs) comprising a given clone.

studies (Kim et al. 2015; Raynaud et al. 2018), *TP53* mutation is an early event, and disruption of the p53 pathway is associated with a high fraction of subclonal mutations. Rather than a hierarchical progression from primary tumor to recurrence, the tumor phylogeny suggests that samples R2 and M originated from more than one clone and developed subclone-specific driver mutations. The branching of clones with high CCF in R2, but negligible CCF in other tumors suggest that tumors R1 and R2 evolved in parallel. In contrast to the monophyletic lineage of R1, R2 is represented in Clones 3 and 11 with comparable CCF. This suggests a spatially heterogeneous distribution of tumor cells, potentially influenced by R2 falling both within and outside of the RT field of R1. The branching pattern of clones with high CCF in tumor M is also suggestive of parallel metastatic events.

DISCUSSION

This young woman had a rapidly progressive sequence of recurrences that is more aggressive than the described pattern of progression in GBM. The sudden and widespread extracranial metastases prompted the clinical team, in discussion with and informed consent from the patient before she died, to undertake further in-depth analysis of the four longitudinal tumor specimens. The presence of common GBM events such as homozygous deletion of *CDKN2A*, *TP53* LOH, 9p loss, high mutational overlap with intracranial gliomas, and positive GFAP staining on histology sections provide strong evidence that the metastasis was derived from the intracranial gliosarcoma, rather than developing independently.

The rarity of cases with extracranial metastases inhibits the elucidation of mechanisms underlying metastatic potential, but studies have suggested that physical barriers inherent to the intracranial environment, such as the dura mater, blood–brain barrier, and limited access to systemic circulation, contribute to the low occurrence of this phenomenon (Harrison et al. 2016; Rosen et al. 2018). Surgical intervention has been implicated as a causative factor in extracranial metastases (Beaumont et al. 2007; Kalokhe et al. 2012; Harrison et al. 2016), but the findings of this study suggest the metastatic behavior observed was inherent to the disease progression rather than induced by therapy. Temozolomide has been found to induce hypermutation and treatment resistance in recurrent tumors (Hunter et al. 2006), but the negligible activity of the TMZ-associated mutational signature in all samples implies that TMZ treatment did not significantly affect the mutational burden of tumors. Only one dose of a PARP inhibitor was given to the patient, but this was given ∼16 mo after the primary tumor diagnosis, and the patient died shortly after, so this likely had a negligible effect as well. Radiotherapy can potentially increase indel mutational burden and induce malignant progression (Behjati et al. 2016), but the decrease of the genome-wide deletion/insertion mutational burden in recurrent intracranial tumors relative to the primary tumor suggests that radiotherapy did not significantly affect the mutational burden of the recurrent tumors.

With this patient, the first recurrent tumor disrupted the dura mater, and involvement of the dura was noted in both intracranial recurrent tumors. Consistent with this behavior, a prior clinical study found dural involvement in 14/19 gliosarcomas analyzed (Dawar et al. 2013). Hematogenous spread via dural veins or spread via cerebrospinal fluid could potentially explain the widespread tumor involvement along the vertebrae observed at the time of the pelvic metastasis. Although outside of the scope of this study, supporting evidence for the inherent metastatic behavior of this patient's tumor could be found through analysis of tumor positive cell-free DNA isolated from blood or cerebrospinal fluid.

The relatively high number of mutations and copy-number alterations in recurrent samples, clonal *TP53* mutations, activity of mutational signatures 3, 8, 16, 21, and 26, and branching phylogeny of these tumors are consistent with behavior previously seen in studies

of genomic instability driving intratumor heterogeneity (Brastianos et al. 2015; Raynaud et al. 2018). A study by Brastianos et al. (2017) analyzed two patients with GBM that metastasized to the lungs, and the tumor phylogeny observed was similar to the branching phylogeny observed in this patient. The proportions of mutations shared by the metastatic tumor and most recent recurrence in those samples (54.54%, 63.11%) was comparable to the proportion shared between tumors R2 and M (52.6%). In that study, a branched "sibling" relationship was observed, in which neither pretreatment nor posttreatment branches were subclonal descendants of each other. In contrast to those cases, here phylogeny and other results suggest that M was of oligoclonal origin, derived partly from R1, and evolved in parallel to R2. This was mirrored in the histopathology findings, in which R2, in contrast with the other tumors, displayed key differences including of loss of GFAP staining in the glial component. This is also consistent with the activity of mutational signature 1, which exhibits clock-like behavior in GBM and other cancers (Alexandrov et al. 2015). Accounting for the rate of somatic accumulation of signature 1 mutations in GBM, the signature activity suggests seeding of M prior to the other tumors, consistent with behavior previously observed (Müller et al. 2014).

CONCLUSION

Here we used genomic analysis of high-resolution WGS data to study a rare case of a gliosarcoma patient with multiple tumor recurrences and an extracranial metastasis. To the best of the authors' knowledge, this is the first analysis of clonal evolution of extracranial metastasis in gliosarcoma. Analyses of somatic mutation and copy-number profiles highlighted a high level of genomic instability in the tumors. Clinically relevant GBM driver events, such as mutations in *TP53*, *NF1*, and *RB1* and deletions in *CDKN2A*, were shared among all tumors. Somatic mutations affecting DNA repair mechanisms coupled with alterations in multiple tumor suppressors contributed to multiple temporally and spatially distinct tumors. The metastatic sample was most similar to R2 with respect to the mutational signature profile, but it was most similar to R1 with respect to the copy-number profile, and the tumor phylogeny suggests that the metastasis was largely derived from R1 as well. Results of the phylogeny suggests that sample M originated from more than one clone, and samples R1 and R2 evolved in parallel. As therapy improves patient outcomes, understanding the mechanisms of GBM progression and metastasis will become more critical. This case study adds supporting evidence to the concept of metastasis as an intrinsic property of GBM, and it highlights the challenges in developing therapies that can effectively target tumor cell populations.

METHODS

DNA Sequencing

DNA was isolated from fresh-frozen tumor sections or whole blood using the DNeasy Blood and Tissue kit (QIAGEN) following the manufacturer's instructions. Libraries were then prepared from the DNA using NEBNext UltraTM DNA Library Prep Kit from Illumina following the manufacturer's instructions. For each sample, 1 µg genomic DNA was randomly fragmented to <500 bp by sonication (Covaris S220). The fragments were treated with End Prep Enzyme Mix for end repairing, 5′phosphorylation and dA-tailing in one reaction, followed by a T-A ligation to add adaptors to both ends. Size selection of adaptor-ligated DNA was then performed using AxyPrep Mag PCR Clean-up (Axygen), and fragments of ~410 bp (with the approximate insert size of 350 bp) were recovered. Each sample was then amplified by PCR for eight cycles using P5 and P7 primers, with both primers carrying

sequences that can anneal with flow cell to perform bridge polymerase chain reaction (PCR) and the P7 primer carrying a six-base index allowing for multiplexing. The PCR products were cleaned up using AxyPrep Mag PCR Clean-up (Axygen), validated using an Agilent 2100 Bioanalyzer (Agilent Technologies), and quantified by Qubit2.0 Fluorometer (Invitrogen).

Then libraries with different indexes were multiplexed and loaded on an Illumina HiSeq instrument according to manufacturer's instructions (Illumina). Sequencing was carried out using a 2 × 150 paired-end configuration; image analysis and base calling were conducted by the HiSeq Control Software (HCS) + RTA 2.7 (Illumina) on the HiSeq instrument. WGS metrics are shown in Supplemental Table 1.

Data Analysis

Sequenced data were aligned to reference sequence build human_g1k_v37_decoy using BWA-mem v0.7.17 (Li and Durbin 2009) and then preprocessed using Picard v2.8.2 (Broad Institute 2019) according to GATK v4.0.12 Best Practices (Van der Auwera et al. 2013). Single-nucleotide variants (SNVs) and indels were detected for individual samples using Mutect2 v4.0.12 (Van der Auwera et al. 2013) with default parameters. BCFtools v1.9 and vt v0.57721 (Tan et al. 2015) were used to sort, left-align, and normalize variants that passed quality filters and decompose multiallelic substitutions into SNVs. SNVs and indels called by MuTect2 were used as a query list for multisample variant calling and genotyping using FreeBayes v1.2.0 (Garrison and Marth 2012). Detected somatic mutations were further filtered by discarding variants with a read depth in any sample of less than 14. Filtered variants were annotated using the Ensembl Variant Effect Predictor (McLaren et al. 2016). Germline SNPs and indels were called using the GATK v4.0.12 germline short variant discovery pipeline (Van der Auwera et al. 2013). Somatic copy-number aberration detection and tumor purity and ploidy estimation were performed using Sequenza v2.1.0 (van Every et al. 2018). Loss of heterozygosity estimation was performed using TitanCNA v1.18.0 (Ha et al. 2014). Structural variant discovery was performed using LUMPY (Layer et al. 2014). Subclonal population reconstruction was performed using phyloWGS (Deshwar et al. 2015). Statistical analyses were performed using R v3.5.1. Mutational signatures were identified using the MutationalPatterns (Blokzijl et al. 2018) R package. Sample mutation rate was defined as the number of somatic mutations present divided by megabases covered.

ADDITIONAL INFORMATION

Data Deposition and Access

Sequencing data will be made available through the European Genome-phenome Archive (EGA) at the time of publication (accession number EGAS00001004076).

Ethics Statement

The patient provided signed informed consent to publication of her clinical data and genomic analysis. This study was approved by the Northern Sydney Local Health District Human Research Ethics Committee (NSLHD HREC).

Acknowledgments

K.C.J. is the recipient of an American Cancer Society Fellowship (130984-PF-17-141-01-DMC). F.P.B. is supported by the JAX Scholar program and the National Cancer Institute (K99 CA226387). The authors thank Sherilyn Goldstone at the NHMRC CTC for her editorial support.

Author Contributions

K.J.A. and A.C.T. equally contributed to the drafting and revision of the manuscript. K.J.A., S.B.A., K.C.J., F.P.B., and R.G.W.V. performed the genomic analysis and interpretation. A.C.T., J.P., M.B., Ma.K., A.N., J.B., H.W., A.L.H., and Mu.K. performed the clinical analysis and interpretation. R.G.W.V. and Mu.K. provided overall guidance to the genomic and clinical analysis and the success of the study.

Competing Interest Statement

R.G.W.V. declares equity in Pretzel Therapeutics. Mu.K. receives research grants from BMS and ABBVie.

Received August 9, 2019; accepted in revised form November 1, 2019.

Funding

This work was supported by the National Brain Tumor Society, Oligo Research Fund; Cancer Center Support grant P30CA034196; and by Cancer Prevention & Research Institute of Texas (CPRIT) grant number R140606 (RGWV).

REFERENCES

Actor B, Cobbers JM, Büschges R, Wolter M, Knobbe CB, Lichter P, Weber RG. 2002. Comprehensive analysis of genomic alterations in gliosarcoma and its two tissue components. *Genes Chromosomes Cancer* **34:** 416–427. doi:10.1002/gcc.10087

Akgül S, Patch A-M, D'Souza RCJ, Mukhopadhyay P, Nones K, Kempe S, Kazakoff SH, Jeffree RL, Stringer BW, Pearson JV, et al. 2019. Intratumoural heterogeneity underlies distinct therapy responses and treatment resistance in glioblastoma. *Cancers (Basel)* **11:** E190. doi:10.3390/cancers11020190

Alexandrov LB, Nik-Zainal S, Wedge DC, Aparicio SAJR, Behjati S, Biankin AV, Bignell GR, Bolli N, Borg A, Børresen-Dale A-L, et al. 2013. Signatures of mutational processes in human cancer. *Nature* **500:** 415–421. doi:10.1038/nature12477

Alexandrov LB, Jones PH, Wedge DC, Sale JE, Campbell PJ, Nik-Zainal S, Stratton MR. 2015. Clock-like mutational processes in human somatic cells. *Nat Genet* **47:** 1402–1407. doi:10.1038/ng.3441

Barthel FP, Wesseling P, Verhaak RGW. 2018. Reconstructing the molecular life history of gliomas. *Acta Neuropathol* **135:** 649–670. doi:10.1007/s00401-018-1842-y

Barthel FP, Johnson KC, Varn FS, Moskalik AD, Tanner G, Kocakavuk E, Anderson KJ, Abiola O, Aldape K, Alfaro KD, et al. 2019. Longitudinal molecular trajectories of diffuse glioma in adults. *Nature* **576:** 112–120.

Beaumont TL, Kupsky WJ, Barger GR, Sloan AE. 2007. Gliosarcoma with multiple extracranial metastases: case report and review of the literature. *J Neurooncol* **83:** 39–46. doi:10.1007/s11060-006-9295-x

Behjati S, Gundem G, Wedge DC, Roberts ND, Tarpey PS, Cooke SL, Van Loo P, Alexandrov LB, Ramakrishna M, Davies H, et al. 2016. Mutational signatures of ionizing radiation in second malignancies. *Nat Commun* **7:** 12605. doi:10.1038/ncomms12605

Bielski CM, Zehir A, Penson AV, Donoghue MTA, Chatila W, Armenia J, Chang MT, Schram AM, Jonsson P, Bandlamudi C, et al. 2018. Genome doubling shapes the evolution and prognosis of advanced cancers. *Nat Genet* **50:** 1189–1195. doi:10.1038/s41588-018-0165-1

Blokzijl F, Janssen R, van Boxtel R, Cuppen E. 2018. MutationalPatterns: comprehensive genome-wide analysis of mutational processes. *Genome Med* **10:** 33. doi:10.1186/s13073-018-0539-0

Brastianos PK, Carter SL, Santagata S, Cahill DP, Taylor-Weiner A, Jones RT, Van Allen EM, Lawrence MS, Horowitz PM, Cibulskis K, et al. 2015. Genomic characterization of brain metastases reveals branched evolution and potential therapeutic targets. *Cancer Discov* **5:** 1164–1177. doi:10.1158/2159-8290.cd-15-0369

Brastianos PK, Nayyar N, Rosebrock D, Leshchiner I, Gill CM, Livitz D, Bertalan MS, D'Andrea M, Hoang K, Aquilanti E, et al. 2017. Resolving the phylogenetic origin of glioblastoma via multifocal genomic analysis of pre-treatment and treatment-resistant autopsy specimens. *NPJ Precis Oncol* **1:** 33. doi:10.1038/s41698-017-0035-9

Broad Institute. 2019. Picard Toolkit. GitHub Repository. Retrieved from http://broadinstitute.github.io/picard/

Ceccarelli M, Barthel FP, Malta TM, Sabedot TS, Salama SR, Murray BA, Morozova O, Newton Y, Radenbaugh A, Pagnotta SM, et al. 2016. Molecular profiling reveals biologically discrete subsets and pathways of progression in diffuse glioma. *Cell* **164:** 550–563. doi:10.1016/j.cell.2015.12.028

Codispoti KE, Mosier S, Ramsey R, Lin MT, Rodriguez FJ. 2014. Genetic and pathologic evolution of early secondary gliosarcoma. *Brain Tumor Pathol* **31:** 40–46. doi:10.1007/s10014-012-0132-y

Colebatch AJ, Witkowski T, Waring PM, McArthur GA, Wong SQ, Dobrovic A. 2018. Optimizing Optimizing amplification of the GC-rich *TERT* promoter region using 7-Deaza-dGTP for droplet digital PCR quantification of *TERT* promoter mutations. *Clin Chem* **64:** 745–747. doi:10.1373/clinchem.2017.284257

Dawar R, Fabiano AJ, Qiu J, Khushalani NI. 2013. Secondary gliosarcoma with extra-cranial metastases: a report and review of the literature. *Clin Neurol Neurosurg* **115:** 375–380. doi:10.1016/j.clineuro.2012.06.017

deCarvalho AC, Kim H, Poisson LM, Winn ME, Mueller C, Cherba D, Koeman J, Seth S, Protopopov A, Felicella M, et al. 2018. Discordant inheritance of chromosomal and extrachromosomal DNA elements contributes to dynamic disease evolution in glioblastoma. *Nat Genet* **50:** 708–717. doi:10.1038/s41588-018-0105-0

Deshwar AG, Vembu S, Yung CK, Jang GH, Stein L, Morris Q. 2015. PhyloWGS: reconstructing subclonal composition and evolution from whole-genome sequencing of tumors. *Genome Biol* **16:** 35. doi:10.1186/s13059-015-0602-8

Garrison E, Marth G. 2012. Haplotype-based variant detection from short-read sequencing. arXiv 1207.3907.

Ha G, Roth A, Khattra J, Ho J, Yap D, Prentice LM, Melnyk N, McPherson A, Bashashati A, Laks E, et al. 2014. TITAN: inference of copy number architectures in clonal cell populations from tumor whole-genome sequence data. *Genome Res* **24:** 1881–1893. doi:10.1101/gr.180281.114

Han SJ, Yang I, Tihan T, Prados MD, Parsa AT. 2010. Primary gliosarcoma: key clinical and pathologic distinctions from glioblastoma with implications as a unique oncologic entity. *J Neurooncol* **96:** 313–320. doi:10.1007/s11060-009-9973-6

Harrison WT, Hulette CM, Guy C, Sporn T, Cummings T. 2016. Metastatic glioblastoma: a case report and review of the literature. *J. Med Surg Pathol* **1:** 1–4. doi:10.4172/2472-4971.1000115

Hunter C, Smith R, Cahill DP, Stephens P, Stevens C, Teague J, Greenman C, Edkins S, Bignell G, Davies H, et al. 2006. A hypermutation phenotype and somatic *MSH6* mutations in recurrent human malignant gliomas after alkylator chemotherapy. *Cancer Res* **66:** 3987–3991. doi:10.1158/0008-5472.CAN-06-0127

Kalokhe G, Grimm SA, Chandler JP, Helenowski I, Rademaker A, Raizer JJ. 2012. Metastatic glioblastoma: case presentations and a review of the literature. *J Neurooncol* **107:** 21–27. doi:10.1007/s11060-011-0731-1

Kim H, Zheng S, Amini SS, Virk SM, Mikkelsen T, Brat DJ, Grimsby J, Sougnez C, Muller F, Hu J, et al. 2015. Whole-genome and multisector exome sequencing of primary and post-treatment glioblastoma reveals patterns of tumor evolution. *Genome Res* **25:** 316–327. doi:10.1101/gr.180612.114

Lawrence MS, Stojanov P, Polak P, Kryukov GV, Cibulskis K, Sivachenko A, Carter SL, Stewart C, Mermel CH, Roberts SA, et al. 2013. Mutational heterogeneity in cancer and the search for new cancer-associated genes. *Nature* **499:** 214–218. doi:10.1038/nature12213

Layer RM, Chiang C, Quinlan AR, Hall IM. 2014. LUMPY: a probabilistic framework for structural variant discovery. *Genome Biol* **15:** R84. doi:10.1186/gb-2014-15-6-r84

Li H, Durbin R. 2009. Fast and accurate short read alignment with Burrows–Wheeler transform. *Bioinformatics* **25:** 1754–1760. doi:10.1093/bioinformatics/btp324

Liu CA, Chang CY, Hsueh KW, Su HL, Chiou TW, Lin SZ, Harn HJ. 2018. Migration/invasion of malignant gliomas and implications for therapeutic treatment. *Int J Mol Sci* **19:** E1115. doi:10.3390/ijms19041115

Luijten MNH, Lee JXT, Crasta KC. 2018. Mutational game changer: chromothripsis and its emerging relevance to cancer. *Mutat Res* **777:** 29–51. doi:10.1016/j.mrrev.2018.06.004

Martincorena I, Raine KM, Gerstung M, Dawson KJ, Haase K, Van Loo P, Campbell PJ. 2017. Universal patterns of selection in cancer and somatic tissues. *Cell* **171:** 1029–1041 e1021. doi:10.1016/j.cell.2017.09.042

McLaren W, Gil L, Hunt SE, Riat HS, Ritchie GR, Thormann A, Cunningham F. 2016. The Ensembl Variant Effect Predictor. *Genome Biol* **17:** 122. doi:10.1186/s13059-016-0974-4

Memmel S, Sisario D, Zöller C, Fiedler V, Katzer A, Heiden R, Becker N, Eing L, Ferreira FLR, Zimmermann H, et al. 2017. Migration pattern, actin cytoskeleton organization and response to PI3K-, mTOR-, and Hsp90-inhibition of glioblastoma cells with different invasive capacities. *Oncotarget* **8:** 45298–45310. doi:10.18632/oncotarget.16847

Müller C, Holtschmidt J, Auer M, Heitzer E, Lamszus K, Schulte A, Matschke J, Langer-Freitag S, Gasch C, Stoupiec M, et al. 2014. Hematogenous dissemination of glioblastoma multiforme. *Sci Transl Med* **6:** 247ra101. doi:10.1126/scitranslmed.3009095

Naumman U, Harter P, Rubel J, Ilina E, Blank A-E, Esteban H, Mittelbronn M. 2013. Glioma cell migration and invasion as potential target for novel treatment strategies. *Transl Neurosci* **4:** 301–329. doi:10.2478/s13380-013-0126-1

Ostrom QT, Gittleman H, Xu J, Kromer C, Wolinsky Y, Kruchko C, Barnholtz-Sloan JS. 2016. CBTRUS Statistical Report: primary brain and other central nervous system tumors diagnosed in the United States in 2009–2013. *Neuro Oncol* **18:** v1–v75. doi:10.1093/neuonc/now207

Parsons DW, Jones S, Zhang X, Lin JC-H, Leary RJ, Angenendt P, Mankoo P, Carter H, Siu I-M, Gallia GL, et al. 2008. An integrated genomic analysis of human glioblastoma multiforme. *Science* **321:** 1807–1812. doi:10.1126/science.1164382

Raynaud F, Mina M, Tavernari D, Ciriello G, Kool M. 2018. Pan-cancer inference of intra-tumor heterogeneity reveals associations with different forms of genomic instability. *PLoS Genet* **14:** e1007669. doi:10.1371/journal.pgen.1007669

Rosen J, Blau T, Grau SJ, Barbe MT, Fink GR, Galldiks N. 2018. Extracranial metastases of a cerebral glioblastoma: a case report and review of the literature. *Case Rep Oncol* **11:** 591–600. doi:10.1159/000492111

Tan A, Abecasis GR, Kang HM. 2015. Unified representation of genetic variants. *Bioinformatics* **31:** 2202–2204. doi:10.1093/bioinformatics/btv112

Taylor AM, Shih J, Ha G, Gao GF, Zhang X, Berger AC, Schumacher SE, Wang C, Hu H, Liu J, et al. 2018. Genomic and functional approaches to understanding cancer aneuploidy. *Cancer Cell* **33:** 676–689.e673.

Van der Auwera GA, Carneiro MO, Hartl C, Poplin R, Del Angel G, Levy-Moonshine A, Jordan T, Shakir K, Roazen D, Thibault J, et al. 2013. From FastQ data to high confidence variant calls: the Genome Analysis Toolkit best practices pipeline. *Curr Protoc Bioinformatics* **43:** 11.10.11–11.10.33. doi:10.1002/0471250953.bi1110s43

Van Every MJ, Dancik G, Paramesh V, Gurda GT, Meier DR, Cash SE, Guin S. 2018. Genomic case report of a low grade bladder tumor metastasis to lung. *BMC Urol* **18:** 74. doi:10.1186/s12894-018-0386-8

Verhaak RGW, Hoadley KA, Purdom E, Wang V, Qi Y, Wilkerson MD, Miller CR, Ding L, Golub T, Mesirov JP, et al. 2010. Integrated genomic analysis identifies clinically relevant subtypes of glioblastoma characterized by abnormalities in PDGFRA, IDH1, EGFR, and NF1. *Cancer Cell* **17:** 98–110. doi:10.1016/j.ccr.2009.12.020

Waite KJ, Wharton SB, Old SE, Burnet NG. 1999. Systemic metastases of glioblastoma multiforme. *Clin Oncol (R Coll Radiol)* **11:** 205–207. doi:10.1053/clon.1999.9045

Weller M, Wick W, Aldape K, Brada M, Berger M, Pfister SM, Nishikawa R, Rosenthal M, Wen PY, Stupp R, et al. 2015. Glioma. *Nat Rev Dis Primers* **1:** 15017. doi:10.1038/nrdp.2015.17